NUMERICAL SIMULATION OF THE RAMOS GAS CONDENSATE RESERVOIR

Hector Quiroga, José Lúquez and Victor Hamdan: Pluspetrol E&P, Bs. As., Argentina
Farhad Sobbi, David Shaw, Douglas W. Bennion and Dave Poon: Hycal, Calgary, Canada

SUMMARY

The Ramos Field is a giant, naturally fractured gas condensate reservoir located in Salta, Northwest Argentina. This field is the biggest discovered to date in the Subandean Belt of Argentina and Bolivia. The field started production in 1979 with one well, and currently is producing 8.7 MM std m^3/D from 10 wells, 3 of them horizontal. The Ramos Field is a very complex reservoir with 5 thick quartzitic sandstone layers. The gas column is 1500 m thick. The fracture system in Ramos was observed during drilling, coring, well testing and in many image logs.

We used a three dimensional, compositional, dual porosity model to simulate the performance of the Ramos Field. The simulation study started in 1993 and continued with field development. The objectives of the simulation were to develop a quantitative reservoir model, simulate the production and pressure history of the field and to optimize the future production strategy.

The simulation input data consisted of geological, petrophysical and well data, production and pressure history, PVT analyses and conventional and special core analyses. Borehole imaging logs, the results of many transient pressure buildups, and an interference test which showed the directions of maximum and minimum permeability were used to construct the fracture permeability distribution maps.

A recombined sample from well R-1004 was used to tune a five pseudo-component equation of state (EOS) using the experimental saturation pressure, the separator test data and the constant volume depletion test (CVD) data. The simulation model was initialized using a gas water contact of -2820 mss and an initial uniform gas composition throughout the reservoir.

The field fracture permeability played an important role in modeling the observed field pressure gradient. In general, the north-south fracture permeability was greater than the east-west fracture permeability. However, the fracture permeability of each well estimated from well test analysis was assigned to the individual wells and the drainage area was changed to produce the best pressure history match. The simulation results show the need for a partially sealing barrier isolating the southern part from the main reservoir.

An excellent well pressure history match was achieved. The history match of well shut-in pressures was also satisfactory. The history match of wellbore condensate flow rate was excellent before 1994. After 1994, the simulation produced slightly more condensate than the actual well production.

Ten predictive runs were conducted in order to optimize the production strategy for the Ramos Field. The objective of the predictive runs was to produce 11MM std m^3/day of gas from the Ramos Field starting in June 1999, and to maintain this field gas flow rate by drilling infill wells and/or installing surface compression to decrease well head pressure.

Analysis of the simulation predictions show that the field ultimate gas recovery is affected by the surface pressure limit. Lower surface pressures produce higher cumulative gas production. The results also demonstrate that the field ultimate cumulative gas production is not affected by additional infill wells. However, the infill wells will maintain the field target gas production rate for a longer period of time.

INTRODUCTION

The Ramos Field is a giant, naturally fractured gas condensate reservoir located in Salta, Northwest Argentina. This field is the biggest discovered to date in the Subandean Belt of Argentina and Bolivia. The field started production in 1979 with one well, and currently is producing 8.7 MM std m^3/D from 10 wells, 3 of them horizontal. The Ramos Field is a very complex reservoir with 5 thick quartzitic sandstone layers. The gas column is 1500 m thick. The fracture system in Ramos was observed during drilling, coring, well testing and in many image logs. The fracture system is mainly due to folding and faulting processes.

We used a three dimensional, compositional, dual porosity model[1, 2, 3, 4] to simulate the performance of the Ramos Field. The simulation study started in 1993 and continued with the field development. The primary objectives of the study were to develop a reservoir model and simulate the production and pressure history of the Ramos Field, and run predictions of the future field performance in order to optimize the production strategy. The objective of the predictive runs was to produce 11 MM std m^3/day of gas from the Ramos Field starting in June 1999, and to maintain this field gas flow rate by drilling infill wells and/or installing surface compression to decrease wellhead pressure. This paper presents the methodology and results of the study.

The Computer Modeling Group's (CMG) compositional simulator GEM was used to simulate the Ramos Field. GEM is a multidimensional EOS compositional simulator, which can simulate all the important mechanisms of the depletion and recycling of a gas condensate in homogeneous or heterogeneous reservoirs.

GEOLOGICAL SETTING

The Ramos Field, located in the Northwestern Basin of Argentina (Figure 1), is the largest gas- and condensate-producing field discovered to date in the entire Subandean Thrust and Fold Belt of Argentina and Bolivia[5].

The stratigraphic column in the Ramos Field area consists of Paleozoic sediments (Silurian-Devonian-Carboniferous) and a lower Cenozoic cover, all affected by Tertiary compressive tectonism[6]. The Silurian-Devonian stratigraphy comprises a succession of alternating pelitic and sandy marine units, which in general can be divided into three prograding sequences. The lowermost Cinco Picachos Supersequence contains Early Devonian Santa Rosa Formation reservoir rocks. The overlying Middle Devonian Las Pavas Supersequence contains the Huamampampa and Icla Formations, the most important gas bearing reservoirs in the Ramos Field (Figure 2). The uppermost Aguarague Supersequence is composed of a thick column of marine shales of the Los Monos Formation, which is the source rock for the gas in the Ramos Field. The depositional environment for the Silurian-Devonian sediments is interpreted as a distal shelf for the shale portion in the lower part of each supersequence, and a shallowing-upwards progradational proximal sandstone facies in the upper part of each supersequence. The Los Monos Formation corresponds to a highstand event at the end of Devonian that is recognized worldwide.

Unconformably overlying the Los Monos Formation are Carboniferous continental fluvio-glacial sediments that were exploited during the early life of the Ramos Field to produce oil from Tupambi and Tarija Formation sandstones and conglomerates. Today, this shallow oil field is abandoned. Tertiary sediments, including syntectonic sandy units whose growth patterns are the key to delineating the timing of Tertiary deformation in the region, form the sedimentary cover in the Ramos Field area.

The Ramos structure, as shown in Figure 3, is formed by two thrusted sheets: one deep with detachment in the Silurian Kirusillas Formation that involved all Devonian units; and another shallower detachment surface in the Los Monos Formation involving Carboniferous and Tertiary rocks that produced the present surface geomorphology to the Ramos area. The structure at the producing levels is a faulted, doubly-plunging, north-northeast elongated anticline, about 20 km long by 4 km wide, located in the central part of the Subandean Thrust and Fold Belt. The geometry of the structure is asymmetrical, with a backlimb dipping about 34 degrees to the west, a moderately wide crest, and a steeply dipping forelimb to the east (more than 60 degrees) containing the most productive open fractures.

Reservoirs are developed in naturally fractured Devonian quartzitic sandstones of the Huamampampa, Icla and Santa Rosa Formations (Figure 4). The reservoirs in the Huamampampa are named, from top to bottom, Units 1, 2A, 2B, 3A, 3B and 3C, while those in the underlying Icla Formation are named Units 5 and 7. These sandstones contain a large number of natural tectonic fractures resulting from the superposition of several compressional events. Most of these fractures are open or partially open tensional fractures (Figures 5 and 6), resulting in very good fracture porosity that controls fluid flow to the wellbores. Fracture porosity reaches a maximum of 2% in the Huamampampa[7] and averages about 0.7%. True matrix porosity is very poor, less than 0.1%, but significant micro-fracture porosity is present and was considered to be matrix porosity in the simulator model. The most intensely fractured zones are located in the forelimb and crestal zone, while fracture density decreases in the backlimb and plunges. Intensive tectonic deformation gave the Ramos anticline its high structural position and an intense fracture system up to 1500 m thick.

Seals in the Ramos structure are thick, deformed Los Monos Formation shales (more than 2000m thick, mainly due to duplex stacking), highly overpressured with gas.

Gas and condensate are the main fluids produced from the Huamampampa and Icla Formations. The underlying Santa Rosa Formation has a volatile oil ring and associated gas cap containing gas and condensate. Middle-Upper Devonian Los Monos Formation marine shales have been identified as the main source of gas and oil in Northwest Argentina and South Bolivia[8]. Hydrocarbon generation and migration began in the Miocene, and today this source rock is still in the oil-window in anticlines and in the gas-window in synclines. Even though it is not a rich source rock, Los Monos Formation has enough thickness (500 to 900m) and a large areal distribution surrounding the anticlines to generate a huge amount of hydrocarbons in the region. Gas moved from Los Monos to the underlying Huamampampa and Icla Formations due to overpressure in the source rocks and normal pressure in the reservoirs. Another important component of the migration system could be the faults occurring in the Ramos anticline[9].

SIMULATOR MODEL CONSTRUCTION

The geological model used for numerical simulation was developed using structural contour maps of the tops of Units 2A, 2B, 3A, 3B and 3C of the Huamampampa Formation, open hole and production logs from 11 wells, results of the interpretation of wellbore imaging logs, core descriptions and core analysis data, and dynamic reservoir data. Unit 1 of the Huamampampa Formation and Units 5 and 7 of the Icla Formation were excluded from the simulation model.

A suite of five full sized structural contour maps consisting of the tops of Units 2A, 2B, 3A, 3B and 3C were digitized and used to construct the simulation model utilizing CMG's Grid Builder software. In the process of construction of the simulation model, local pinch out of some layers was observed. The thickness of each pinched out grid block was corrected by carefully examining the thickness of adjacent grids and assigning a thickness within the limits of the minimum and maximum thickness of the layer in the area under consideration. All grids having a thickness smaller than the minimum observed thickness in each layer were set to the minimum thickness, and all grids having a thickness larger than the maximum observed thickness were set to the maximum thickness. Units 2A and 2B were sub-divided into two layers each, so the final simulator model contains 11 layers in the vertical direction as shown in Table 1.

The matrix porosity and fracture porosity maps of Units 2A, 2B, 3A, 3B and 3C were digitized and used to distribute porosity in the two systems of the dual porosity simulation model. The distributed porosity was then modified. All porosity values less than one percent were made equal to one percent. From core analysis data, a relationship between matrix porosity and matrix permeability was developed and used to distribute matrix permeability. The matrix permeability was assumed to be isotropic.

A grid-block center grid system of 28 × 88 × 11 cells was employed for the study. All cells were 150 meters by 300 meters in areal dimension, with a variable thickness.

Experimental gas-oil and water-oil relative permeability data and drainage and imbibition capillary pressure data were used in the simulation model. The mercury injection capillary pressure data were converted to a reservoir condition water-gas system. The capillary pressure data was then shifted to an irreducible water saturation of 20.8 %, as measured in the relative permeability test.

FRACTURE PROPERTIES

The core analysis data from wells R-1005 and R-1007 and the analysis of an FMS log run in well R-1007 were studied carefully to estimate fracture spacing. An average major fracture spacing of 25 meters was used, and the effect of horizontal and vertical variations of the fracture spacing on the simulation results was studied during the course of history match. The effect was negligible.

The field fracture permeability played an important role in modeling the observed field pressure gradient. In general, the north south (simulation model y direction) fracture permeability is greater than the east west (simulation model x direction) fracture permeability. The global field fracture permeability in the x direction was 165 md and in the y direction was 265 md, and the vertical fracture permeability was 6.4 md. The two horizontal fracture permeabilities were also considered to be history matching parameters. The fracture permeability of each well estimated from well test analysis[10, 11] was assigned to each individual well, and the well's drainage area was changed to produce the best pressure history match. Some of the wells did not follow this rule, therefore their permeability was changed to produce the best pressure match. Table 2 compares the well test fracture permeability with the simulation fracture permeability for each well.

A partial communication boundary was placed between the Ramos Field and the Porcelana Field to the southwest of Ramos. This boundary, which approximately follows the southern limit of the Ramos Field, was critical in matching the field pressure measurements and was further confirmed with the geological observation of an overthrust fault in that area. However, the necessary degree of communication between well R-1008 Horizontal and R-1009 was provided through a window in the east side of the field.

Straight-line fracture relative permeability curves and a gas-oil capillary pressure of zero in the fractures were assumed. Sensitivity analysis of the simulation results using a variety of capillary pressure values in the fracture system showed that, for this reservoir, gas-oil capillary pressure does not affect recovery. A 5% water saturation was used for the fractures, and the water-oil capillary pressure was set to zero.

FLUID PROPERTIES

A recombined sample from well R-1004 was selected to tune an equation of state (EOS) using the experimental saturation pressure, separator test data and constant volume depletion test (CVD) data. Fourteen components were used to do the initial fitting: the components were N_2, CO_2, C_1, C_2, C_3, iC_4, nC_4, iC_5, nC_5, C_6, C_7, C_8, C_9, and C_{10+}. The CVD data, saturation pressure and separator test data were used to fit a Peng-Robinson's equation of state[12]. The equation was tuned to the experimental data by adjusting the interaction parameter between C_1 and C_{10+}. The critical properties and molecular weight of C_{10+} were also adjusted. A non-linear regression option was used to fit the experimental data

For the numerical simulation, the 14 components were lumped into 5 pseudo-components in order to keep the computational time and required computer memory size reasonable.

The two equations of state were used with a compositional single well radial model in order to compare their properties under reservoir and surface conditions for a significant reservoir pressure drop. The match between the simulation results using the two equations of state was excellent, therefore the 5 pseudo-component EOS was used to model the fluid flow behavior in the reservoir.

.

The gas/water contact established by field observations at -2820 mss was used to initialize the model. Initial reservoir fluid volumes and pressures are shown in Table 3.

FIELD HISTORICAL DATA

Each well's static pressure history corrected to a datum of -1900 mss was used for the purpose of a pressure history match. The pressure data shows a field-wide slow pressure decline with good reservoir connectivity. An initial reservoir datum pressure of 30819 KPa was used in the simulator.

The monthly gas production was used to calculate an average gas flow rate for each well in each month of the production history. These gas rates were used as input to the simulator. The historical condensate and water production was used to calculate average monthly flow rates for history matching purposes.

HISTORY MATCHING

The main emphasis of the history matching was to match the reported static pressure for each well. In the simulation, the well static pressure measurements were compared to the grid block pressure of the block containing the well. Pressures in all grid blocks opened to a well were averaged and corrected to the datum of -1900 mss.

The horizontal fracture permeability was the main parameter adjusted to match the reservoir pressure. A global fracture permeability in the x direction of 165 md, a fracture permeability in the y direction of 265 md and a vertical fracture permeability of 6.4 md produced the best overall field results. In order to match individual well pressures, a local fracture permeability and drainage area was assigned to each well.

Numerous simulation runs were also conducted to investigate the effects of matrix block size, aquifer activity, and vertical fracture permeability. Matrix block sizes of 5 to 200 meters and vertical fracture permeabilities of 6.4 to 100 md were examined. The effects of matrix block size and vertical fracture permeability on pressure were negligible.

Figure 7 compares the simulator average reservoir pressure corrected to a datum of -1900 mss to the measured reservoir pressures. Figure 8 displays the history match of the field condensate flow rate. The history match of wellbore condensate flow rate is excellent until 1994. After 1994, the simulator produced more condensate than the actual well production.

A comparison of the calculated well block pressure with the measured static pressures for well R-1004 is shown in Figure 9. In all of the wells there is a good agreement between calculated and measured wellbore pressures.

The gas production rate was input in to the simulation model. Figure 10 shows the gas flow rate history match for well R-1004.

The wellbore condensate flow rate history match for well R-1004 is depicted in Figure 11. There is an excellent match at early times for all of the wells. After 1994 the simulator produced more condensate than the actual well production

PREDICTION OF FUTURE FIELD PERFORMANCE

A total of ten predictive runs were conducted to optimize the production strategy for the Ramos Field. A well head pressure constraint was utilized, and skin factors calculated from transient well test analysis were used for each of the wells. Well pressure measurements were used to examine the accuracy of the simulator's wellhead pressure calculation. In general the calculated well head pressures were in good agreement with measured well head pressures.

The objective of the simulation predictive runs was to produce 11 MM std m^3/day of gas from the Ramos Field starting in June 1999, and to maintain this field gas flow rate by drilling infill wells and/or decreasing wellhead pressure by installing surface compression. The simulator output was then used for economic evaluation of alternative production strategies.

The simulation predictive runs consisted of: five predictive runs with well R-12 replaced with a horizontal section put on production with a gas rate of 680,000 std m3/day and well head pressures of 200, 3447, 6894, 8274, and 8963 KPa respectively; three predictive runs with well R-12 producing at 500,000 std m3/day and well head pressures of 200, 1034 and 8274 KPa respectively; one predictive run with well R-12 shut-in and a well head pressure of 8274 KPa; and one predictive run having well R-12 put on production with a gas rate of 500,000 std m3/day, a well head pressure of 8274 KPa and two new infill wells (R-1011 and R-1012).

DISCUSSION

Figure 12 compares the Ramos Field total gas production rate for predictive runs 3 and 6 with predictive run 10. In predictive run 3, with a surface pressure constraint of 8963.2 KPa (1300 psia), the gas rate starts declining before 2003. As can be seen from prediction 6 with a surface pressure constraint of 6894 KPa (1000 psia), the gas rate remains constant until the year 2004. Adding two new infill wells (predictive run 10) maintains the Ramos Field gas production rate constant until the year 2006.

Figure 13 compares the Ramos Field total gas production rate for predictive runs 1 and 8 with predictive run 10. In predictive run 1, with a surface pressure constraint of 200 KPa (29 psia), the gas rate behavior is similar to prediction 8 with a surface pressure of 1034 KPa (150 psia). The difference between the gas production rate of prediction 7 (not shown) with a surface pressure of 3447 KPa (500 psia) and prediction 8 with a surface pressure of 1034 KPa is very small. The gas rate behavior (duration of constant target production rate) in cases 1, 2, 7 and 8 is better than in prediction 10.

The surface pressure in predictions 9 and 10 is equal to 8274 KPa. The simulation predictive run 10 produces with the constant desired target rate of 11 MM std m3/day for about 2 years longer than prediction 9. A full comparison of the Ramos Field gas production rates of predictions 1 to 10 from the year 2009 to 2011 is shown in Figure 14.

Figure 15 compares the cumulative gas and condensate production of the ten simulation predictive runs for the period 1999/07/01 to 2027/01/01. As can be seen the ultimate gas recovery is affected by the surface pressure limit. Lower surface pressures produce higher cumulative gas production. Simulation predictions 4, 5, 9 and 10 with equal surface pressure constraints have equal cumulative gas and condensate production. Predictions 1, 2 and 8 also have similar cumulative gas and condensate production. The two new infill wells in simulation prediction 10 had no effect on ultimate cumulative gas production compared to predictive run 9. However, the two new infill wells maintain the field target gas production rate for an additional period of about 2 years. The difference between simulation predictive runs 7 and 8 is very small. The cumulative gas and condensate production of these two cases compares very well with cases 1 and 2 where the surface pressure is only 200 KPa.

CONCLUSIONS

1. A compositional dual porosity model was used to simulate the performance of the Ramos gas condensate Field.

2. The production and pressure histories of about 20 years were used to history match the simulator model. Fracture permeability in the x and y directions were the main factors affecting the pressure gradient in the Ramos Field. The results of an interference test and many pressure buildup tests were used to adjust the model during the process of history matching the static wellbore pressures. An excellent history match of the static wellbore pressures was achieved.

3. Ten simulation predictive runs were conducted in order to optimize the production strategy for the Ramos Field.

4. Studying the saturation and pressure distribution maps at the time of completion of new wells optimized the location of two infill wells.

5. The field ultimate gas recovery is affected by the surface pressure limit. Lower surface pressures produce higher cumulative gas production.

6. The ultimate cumulative gas production is not affected by new infill wells. However, the new infill wells will maintain the target field gas production rate for a longer time period.

7. The simulation prediction results helped us to rearrange the production schedule in order to uniformly produce the reservoir and optimize the liquid hydrocarbon phase recovery.

8. The start of the gas compression and the amount of gas to be compressed were estimated from the simulation prediction results.

TECHNICAL CONTRIBUTIONS

This case study illustrates the complexities involved in producing naturally fractured gas condensate reservoirs and optimizing the production strategy. It describes the importance of determining fracture permeability when history matching a simulator model of a naturally fractured reservoir. It also demonstrates a procedure for the optimization of infill well locations and the time when they have to be put on production, based on simulation results including spatial gas saturation and reservoir pressure distribution.

REFERENCES

1. Kazemi, H., Vestal, C.F., and Dean Shank, G.: "An Efficient Multicomponent Numerical Simulator," Soc. Petrol. Eng. J., Vol. 18, 1978, pp. 355-368.

2. Gilman, J.R. and Kazemi, H.: "Improvement in Simulation of Naturally Fractured Reservoirs," (Tech. Paper SPE 10511) SOEJ, August 1983, 695-707.

3. Graue, D.J., and Larsen, W.: "Ramos Field: Feasibility of Gas Cycling, An Integration of Geology and Engineering", paper SPE 23649 presented at the Second Latin American Petroleum

Engineering Conference, II LAPEC, of the Society of Petroleum Engineers held in Caracas, Venezuela, March 8-11, 1992.

4. Bennion, D.W., Shaw, D.R., Thomas, F.B., and Bennion, D.B.: "Compositional Numerical Modeling in Naturally Fractured Reservoirs," presented at the 47th Annual Technical Meeting of the Petroleum Society of CIM, June 10-12, 1996, Calgary, Alberta, Canada.

5. Gomez Omil, R. and Luquez, J.: "Ramos Field, a Giant Gas Field in a Subandean Belt (NW Argentina)," 1998 A.A.P.G. International Conference & Exhibition, Rio de Janeiro, Abstracts, 1998, pp. 986-987.

6. Starck, D.: "Silurian-Jurassic Stratigraphy and Basin Evolution of Northwestern Argentina," In: "Petroleum Basins of South America," A.A.P.G. Memoir 62, 1995, pp. 241-267.

7. Sanguinetti, M., Luquez, J. and Clivio, J.: "Fracture Analysis of Paleozoic Sandstones in Ramos field, Northwest Argentina," 1998 A.A.P.G. International Conference & Exhibition, Rio de Janeiro, Abstracts, 1998, pp. 492-493.

8. Disalvo, A. and Villar, H.: "Los Sistemas Petroliferos del Area Oriental de la Cuenca Paleozoica Noroeste, Argentina," IV Congreso de Exploracion y Desarrollo de Hidrocarburos, Mar del Plata, 1999, pp. 83-100.

9. Starck, D.: "Los Sistemas Petroleros de la Cuenca de Tarija," IV Congreso de Exploracion y Desarrollo de Hidrocarburos, Mar del Plata, 1999, pp. 63-82.

10. Stewart, G. and Ascharssobbi, F.: " Well Test Interpretation for Naturally Fractured Reservoirs", paper SPE 18173 presented at the 63 rd Annual Technical Conference and Exhibition of SPE, Houston, Texas, Oct. 2-5, 1988.

11. Quiroga, H., Mellado García, J., Luquez, J. and Alvarado, R.: "Characterizing a Naturally Fractured High Transmissibility Gas Reservoir by Pressure Transient Test," III Latin American/Caribbean Petroleum Engineering Conference, Buenos Aires, 1994, pp. 1215-1228.

12. Peng, D.Y., and Robertson, D.B.: "A New Two-Constant Equation of State," Ind. Eng. Chem. Fundam., Vol. 15, 1976, pp. 59-64.

LIST OF TABLES

Table 1 - Ramos Simulation Model, Names of Layers.
Table 2 - Comparison of Well Test Fracture Permeability with Simulation Fracture Permeability.
Table 3 - Ramos Simulation Model Initial Reservoir Fluid Volumes and Pressures.

LIST OF FIGURES

Figure-1 - Location of the Ramos Field.
Figure 2 - Outcrop of the Huamampampa Formation.
Figure 3 - Ramos Field, Cross-Sections.
Figure 4 - Ramos Field, Type Log.
Figure 5 - Ramos Field, Whole Core Sample Showing an Open Tension Fracture.
Figure 6 - Ramos Field, Typical Image Log Showing Natural Fractures.
Figure 7 - Ramos Field Pressure History Match.
Figure 8 - Ramos Field Condensate Production Rate History Match.
Figure 9 - Well's Pressure History Match for Well R-1004.
Figure 10 - Gas Flow Rate History Match for Well R-1004.
Figure 11 - Condensate Flow Rate History Match for Well R-1004.
Figure 12 - Comparison of Ramos Field Gas Production Rate, Predictive runs 3, 6 and 10.
Figure 13 - Comparison of Ramos Field Gas Production Rate, Predictive runs 1, 8 and 10.
Figure 14 - Comparison of Ramos Field Gas flow Rate from 2009 to 2011.
Figure 15 - Comparison of additional cumulative gas and condensate production from 1999 to 2027, Predictive runs 1 to 10.

TABLE 1

Ramos Simulation Model - Names of Layers

Layer Number	Unit	Lithology	Simulation Model Layer Name and Thickness
1	2A	Sand	2A (Upper), 30 meters
2	2A	Sand	2A (Lower), variable thickness
3	2A	Shale	Shale Layer 1 , 17.4 meters
4	2B	Sand	2B (Upper), 50 meters
5	2B	Sand	2B (Lower), variable thickness
6	2B	Shale	Shale Layer 2, 14.4 meters
7	3A	Sand	3A, variable thickness
8	3A	Shale	Shale Layer 3, 12.8 meters
9	3B	Sand	3B, variable thickness
10	3B	Shale	Shale Layer 4, 17.1 meters
11	3C	Sand	3C, 10 meters

TABLE 2
Comparison of Well Test Fracture Permeability
With Simulation Fracture Permeability

Well Name	Well Test Fracture Permeability, md	Simulation Fracture Permeability, md
R-1001	8.28	200.00
R-1002	165.00	165.00
R-1004	236.00	236.00
R-1005	135.00	135.00
R-1006H3	-	2.20
R-1007	84.76	18.00
R-1009	26.32	26.32
R-11	18.00	18.00
R-12	6.30	150.00
R-15	6.40	200.00

TABLE 3
Ramos Simulation Model
Initial Reservoir Fluid Volumes and Pressures

Initial Reservoir Conditions		Entire Field
Total Pore Volume	MM res m^3	878.78
Total Pore Volume	MM res m^3	493.22
Original Oil in Place, OOIP		
In Oil Zone	MM std m^3	0.0
Condensate in Gas Zone	MM std m^3	0.0
Dissolved in Water Zone	MM std m^3	0.0
Total OOIP	MM std m^3	0.0
Original Gas in Place, OGIP		
In Oil Zone	MMM std m^3	124.43
Dissolved Gas in Oil Zone	MMM std m^3	0.0
Dissolved Gas in Water Zone	MMM std m^3	0.0
Total OGIP	MMM std m^3	124.43
Original Water in Place	MM std m^3	388.62
Average Pressure	KPa	32882.6
Average Porosity	fraction	0.0378
Average Saturations		0.0
Oil %		0.56125
Gas %		0.43875
Water %		

Figure 1

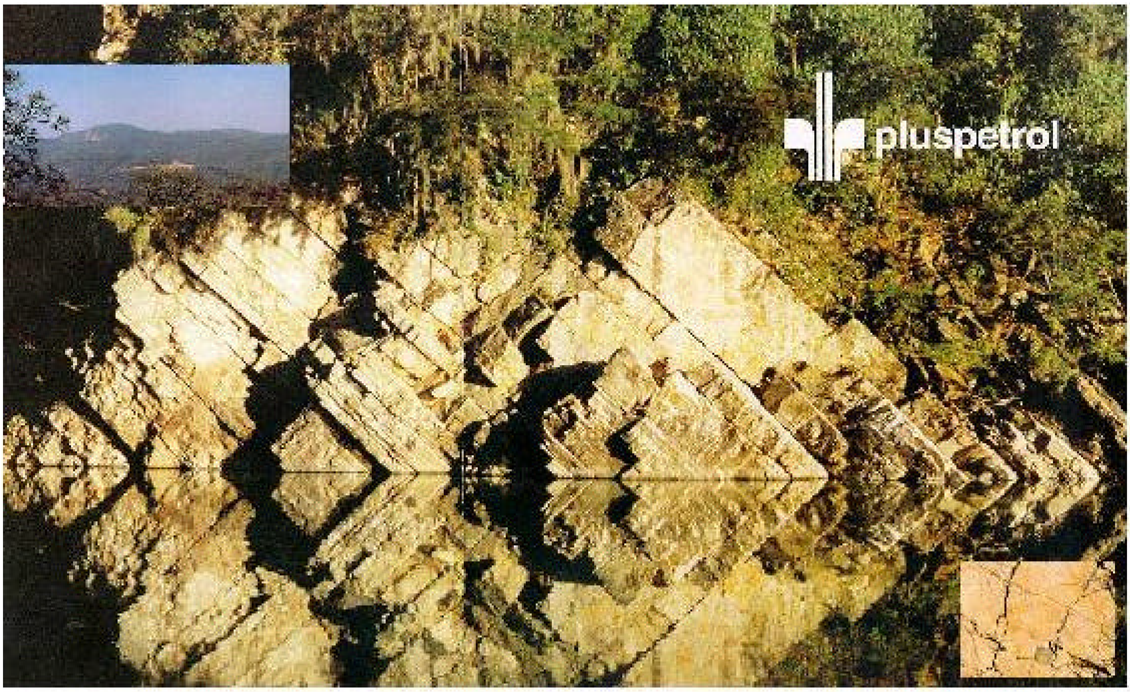

Figure 2

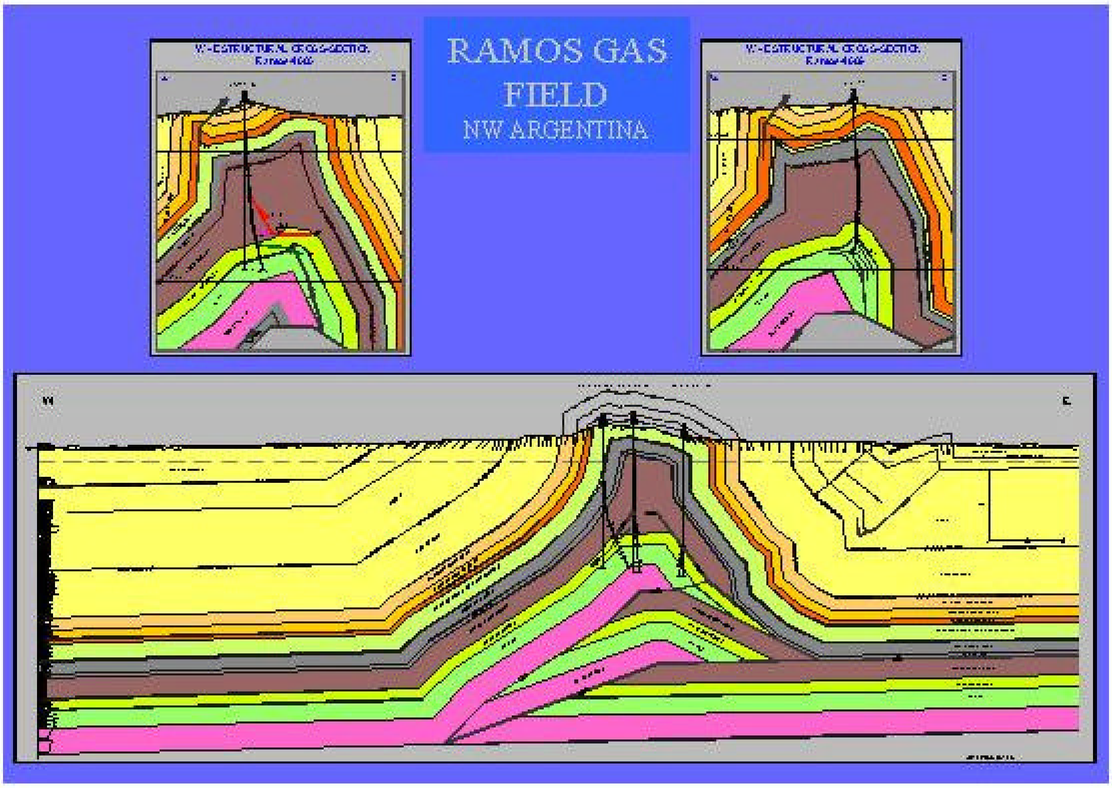

Figure 3

Type well - Rxp11

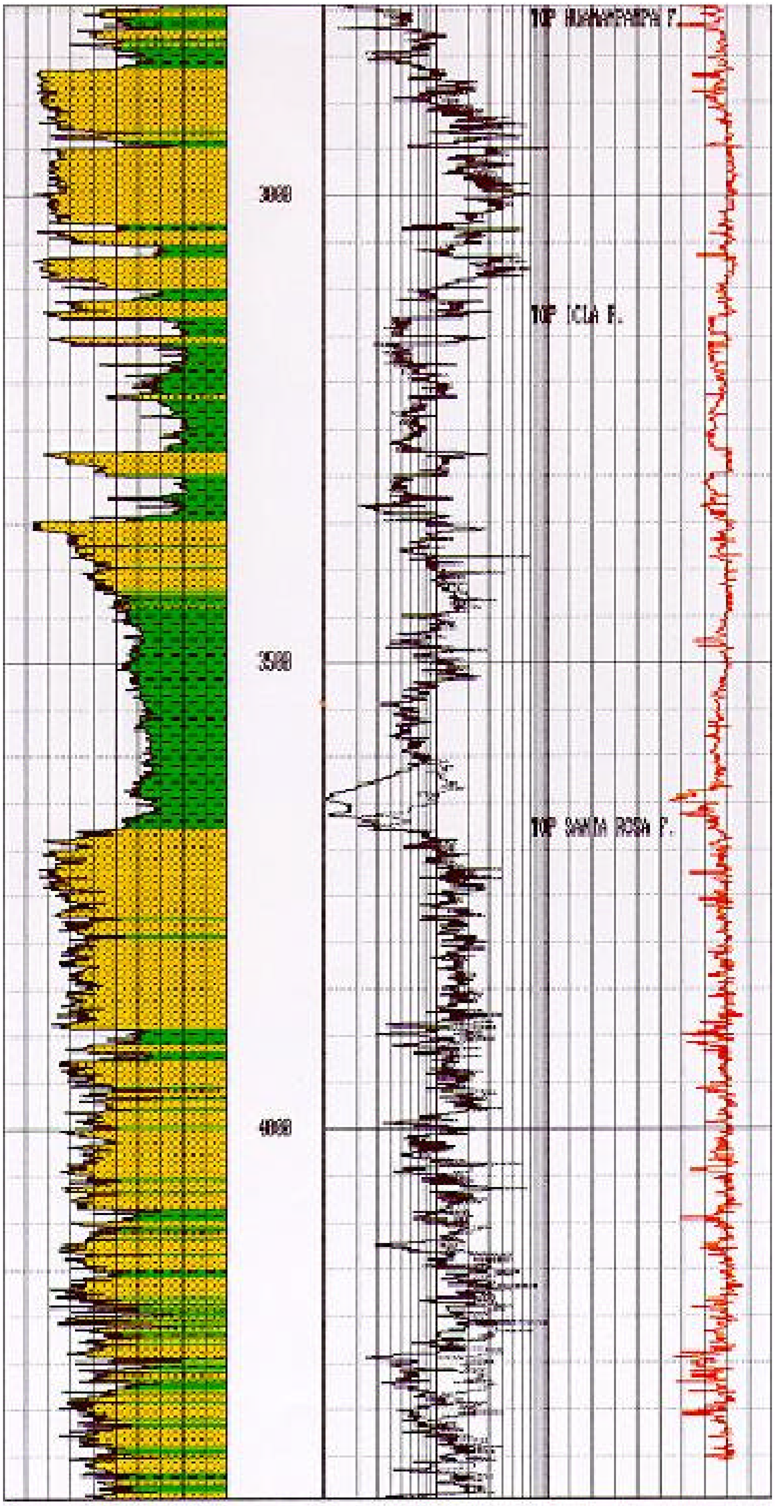

Figure 4

Figure 5

Figure 6

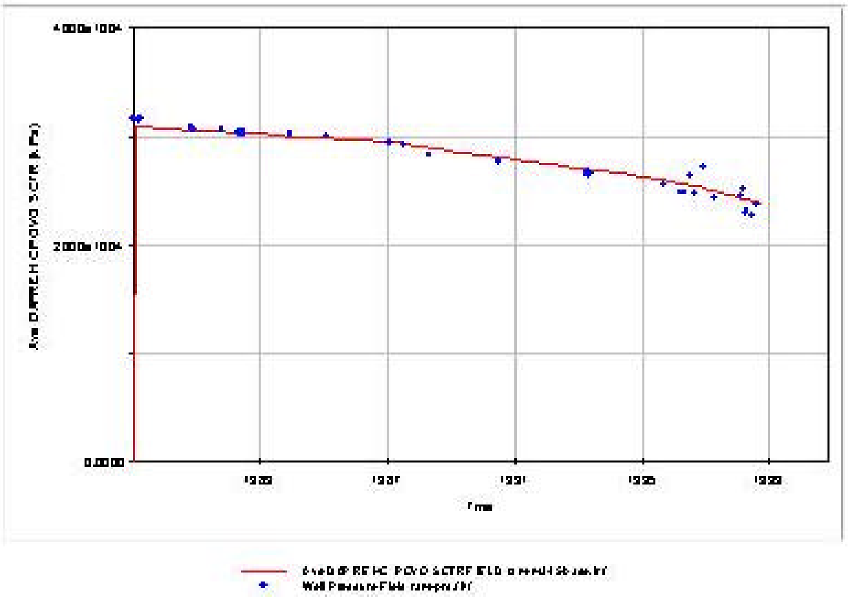

Figure 7

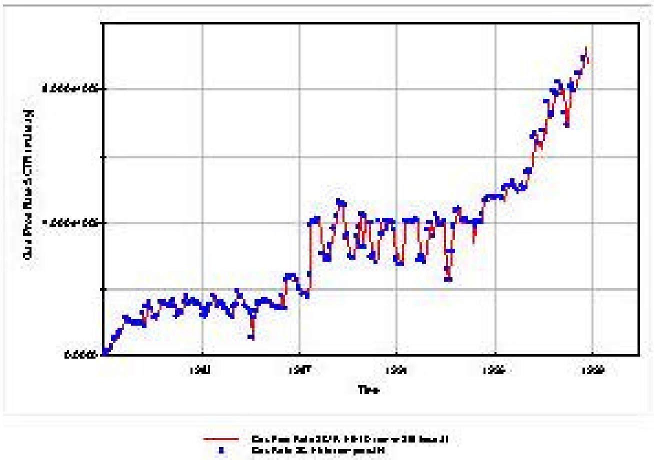

Figure 8

R-1004

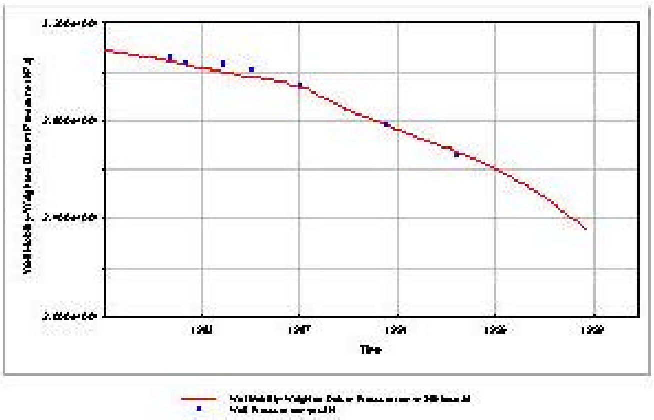

Figure 9

R-1004

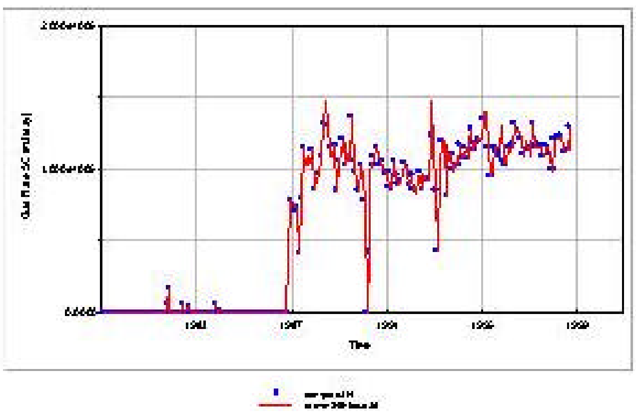

Figure 10

R-1004

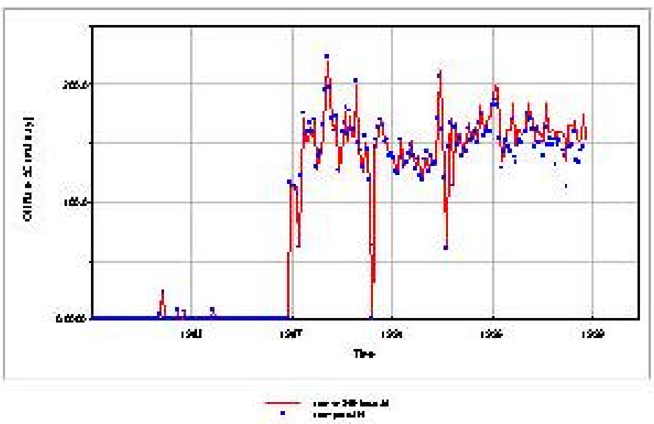

Figure 11

Simulation Prediction - Comparison of Ramos Gas Rate of Production

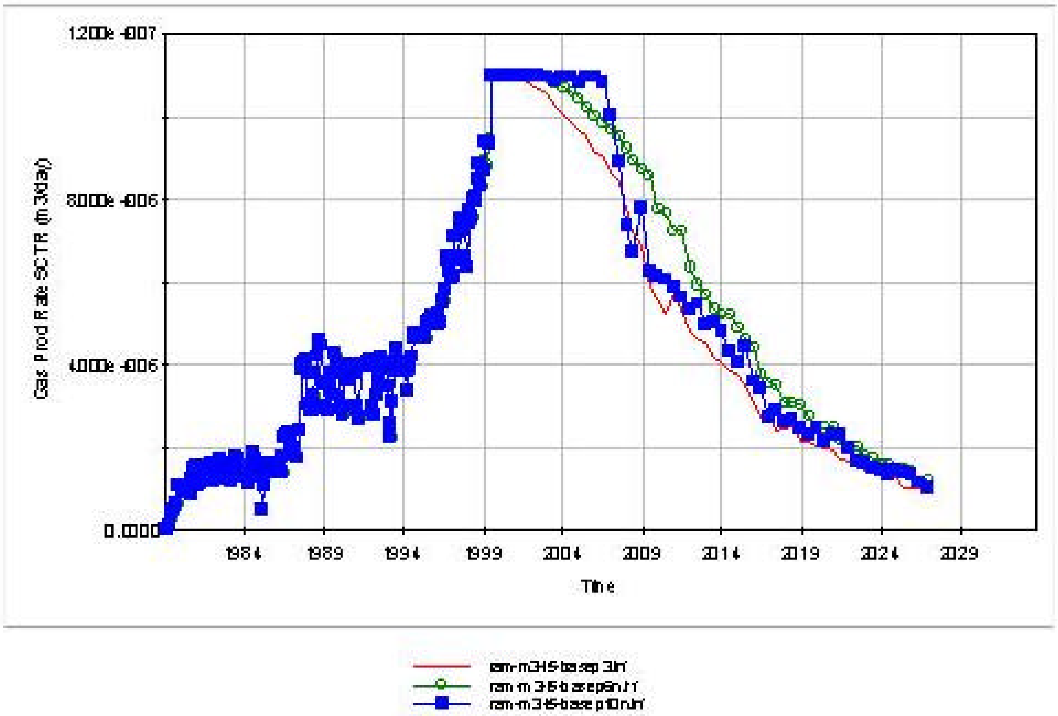

Figure 12

Simulation Prediction - Comparison of Ramos Gas Rate of Production

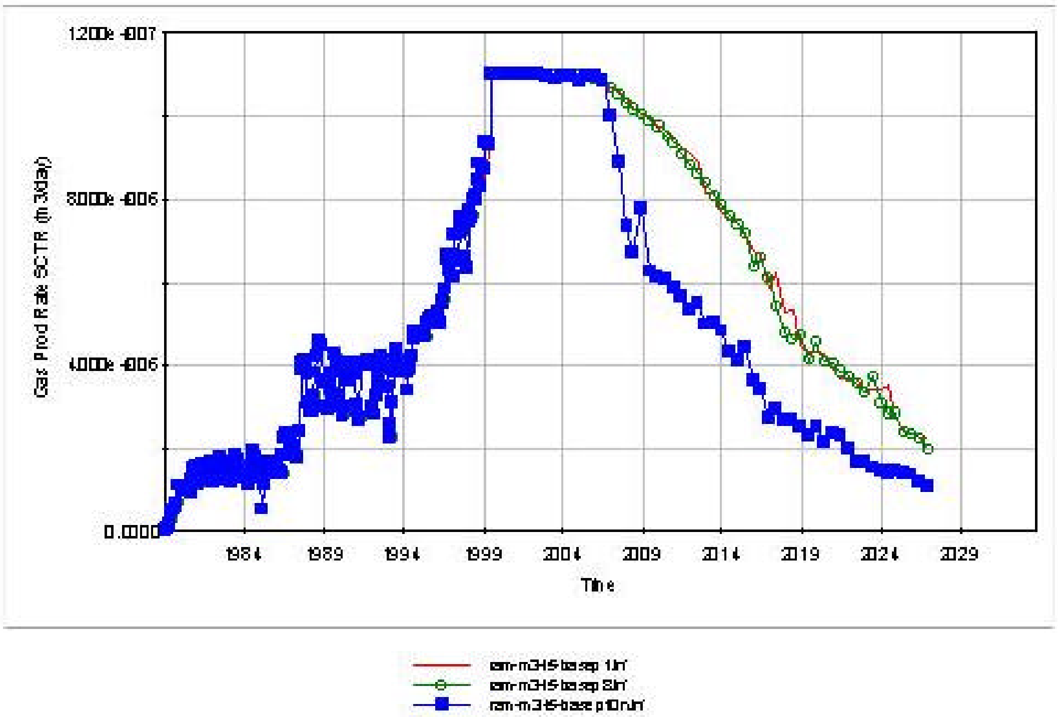

Figure 13

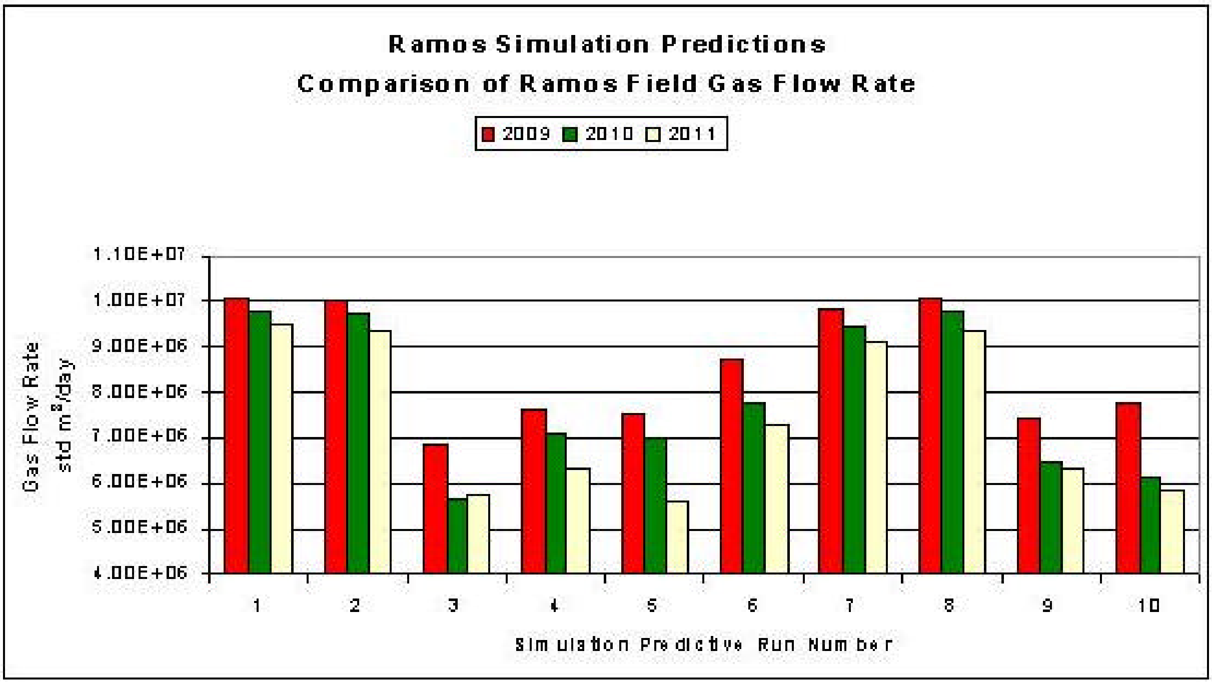

Figure 14

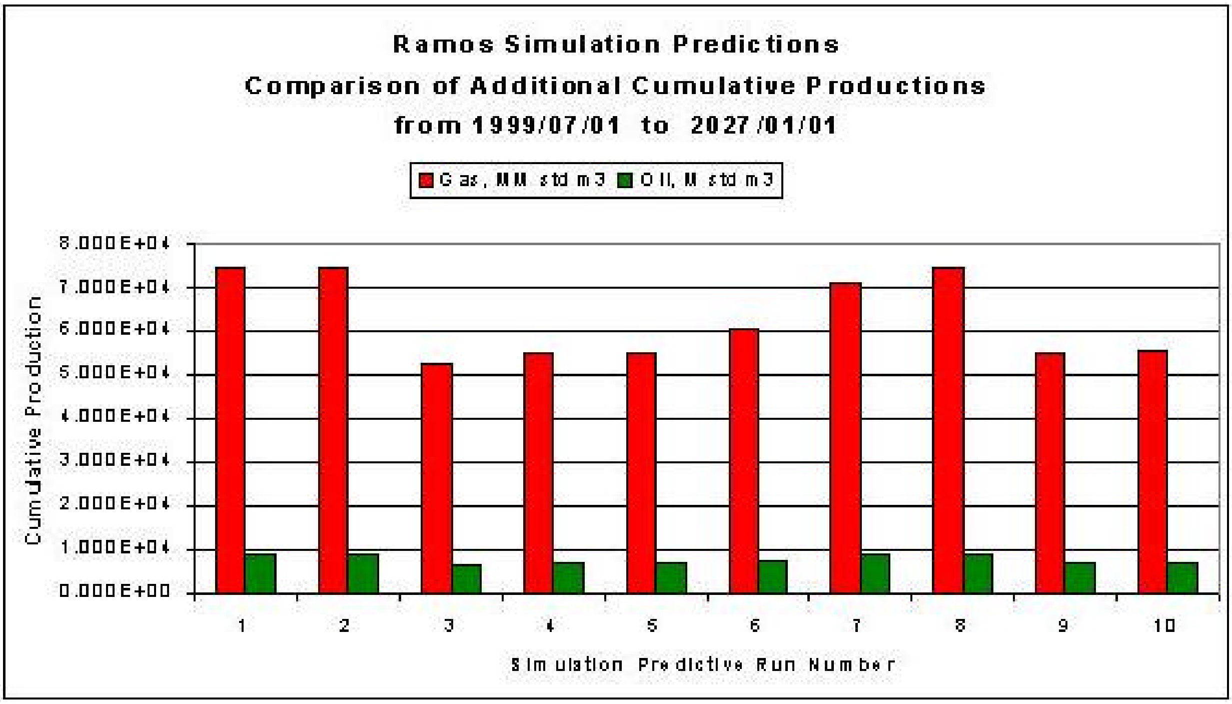

Figure 15